Supporting Information for

Controllable synthesis of polydopamine nanoparticles in microemulsions with pH-activatable properties for cancer detection and treatment

Fuyao Liu,[a,d] Xiuxia He,[c] Junping Zhang,[c] Hongda Chen,[a] Huimao Zhang[,b] and Zhenxin Wang*[,a]*

[a.] State Key Laboratory of Electroanalytical Chemistry, Changchun Institute of Applied Chemistry, Chinese Academy of Sciences, Changchun, 130022, P. R. China.

[b.] Department of Radiology, The First Hospital of Jilin University, Changchun, 130021, P. R. China.

[c.] School of Life Science and Technology, Changchun University of Science and Technology, Changchun, 130022, P. R. China.

[d.] University of Chinese Academy of Sciences, Beijing, 100039, P. R. China.

Additional Fig. S1-S20

Additional Table S1-S2

Additional Fig. S1-S20

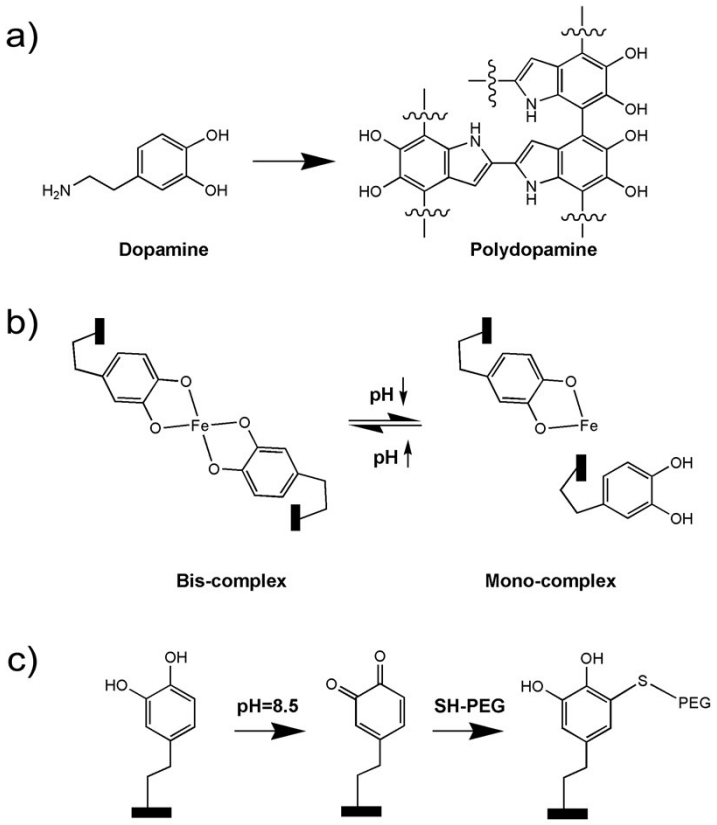

Fig. S1. Schematic illustration of (a) the structure of dopamine and PDA; (b) the coordination between Fe and PDA; (c) the binding pattern of PEG-SH to NPs.

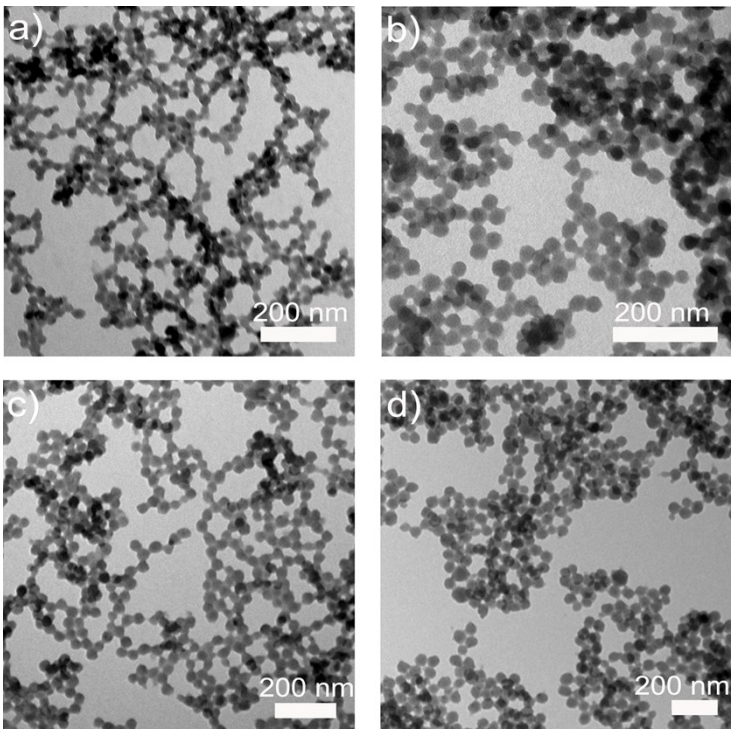

Fig. S2. TEM micrographs of PDA NPs (a) 29 ± 3.3 nm in diameter, obtained with 15 μL of dopamine solution; (b) 34 ± 2.8 nm in diameter, obtained with 30 μL of dopamine solution; (c) 38 ± 3.4 nm in diameter, obtained with 60 μL of dopamine solution; and (d) 43 ± 2.3 nm in diameter, obtained with 120 μL of dopamine solution, respectively.

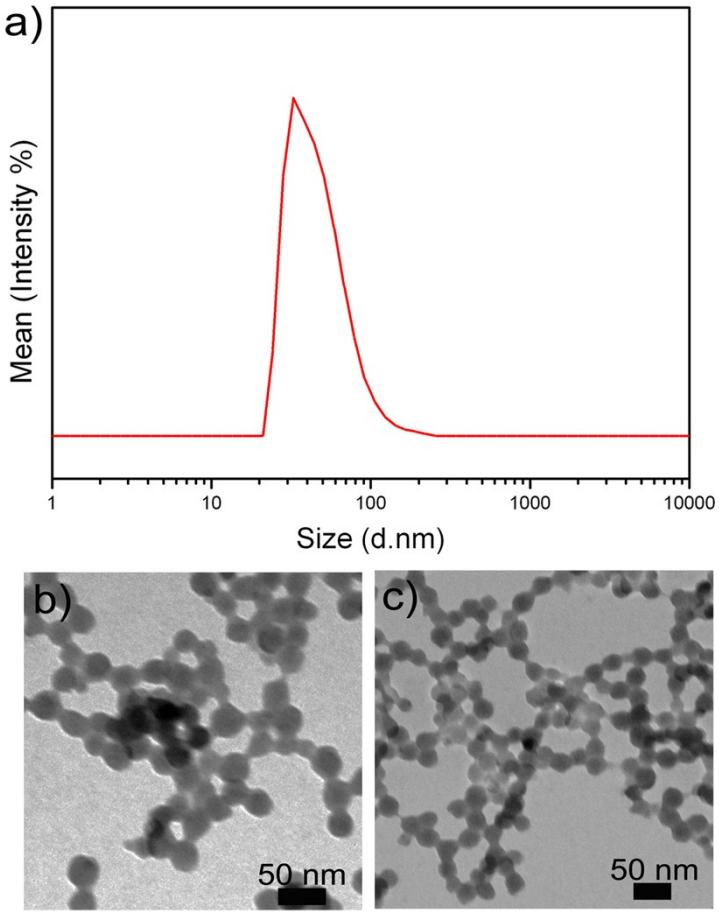

Fig. S3. (a) DLS measurement of PEG-Fe-PDA NPs. TEM micrograph at higher magnification of (b) PDA NPs (25 ± 2.0 nm in diameter, obtained with 7.5 μL of dopamine hydrochloride aqueous solution) and (c) PEG-Fe-PDA NPs, respectively.

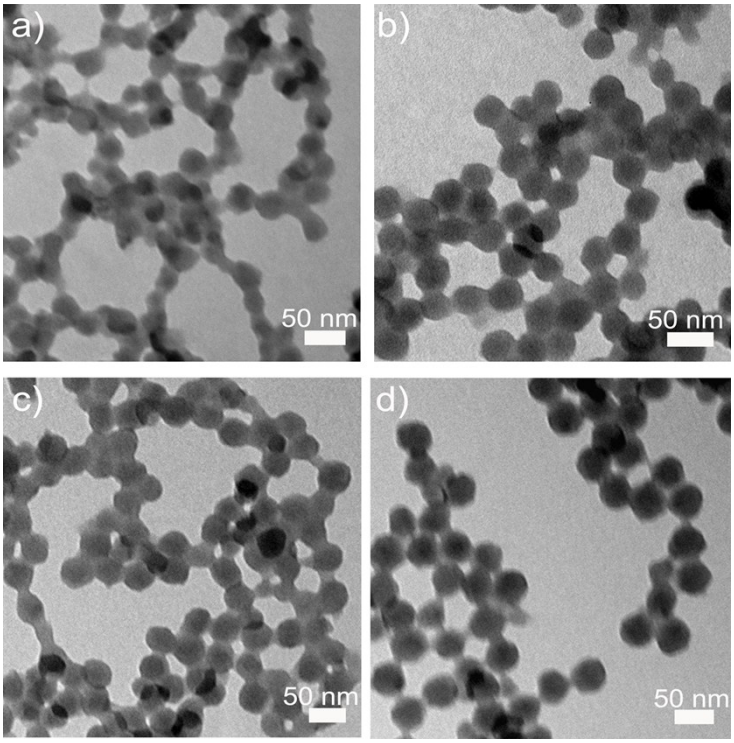

Fig. S4. TEM micrographs at higher magnification of PDA NPs (a) 29 ± 3.3 nm in diameter; (b) 34 ± 2.8 nm in diameter; (c) 38 ± 3.4 nm in diameter; and (d) 43 ± 2.3 nm in diameter, respectively.

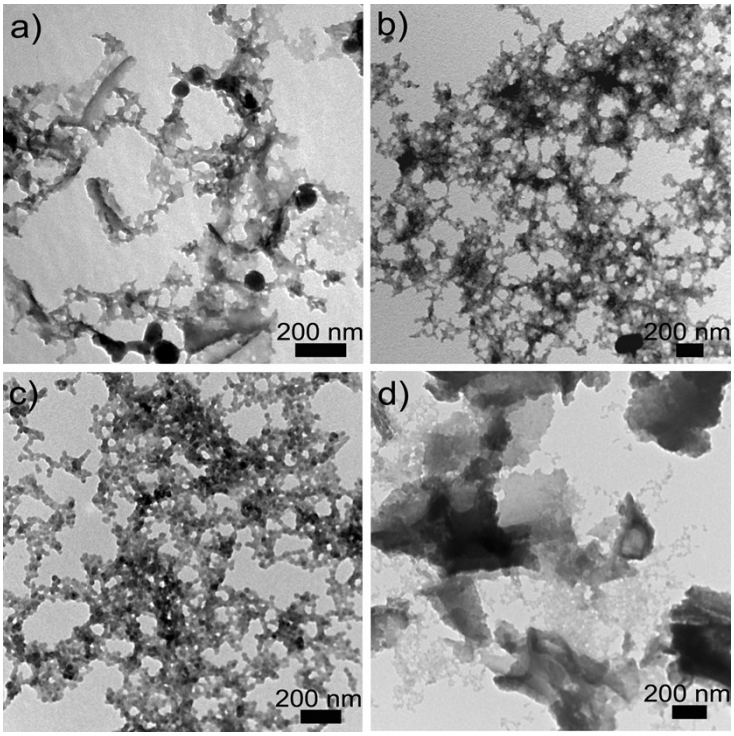

Fig. S5. TEM micrographs of PDA NPs (a) obtained with 40 μL of ammonium hydroxide; (b) obtained with 160 μL of ammonium hydroxide; (c) obtained with reaction temperature of 10 ºC; and (d) obtained with reaction temperature of 50 ºC.

To examine the effect of synthetic parameters, the amount of ammonium hydroxide and the reaction temperature were varied systematically. From the standard synthetic conditions described above, the amount of ammonium hydroxide ranged from 40 to 160 μL and reaction temperature ranged from 10 to 50 ºC.

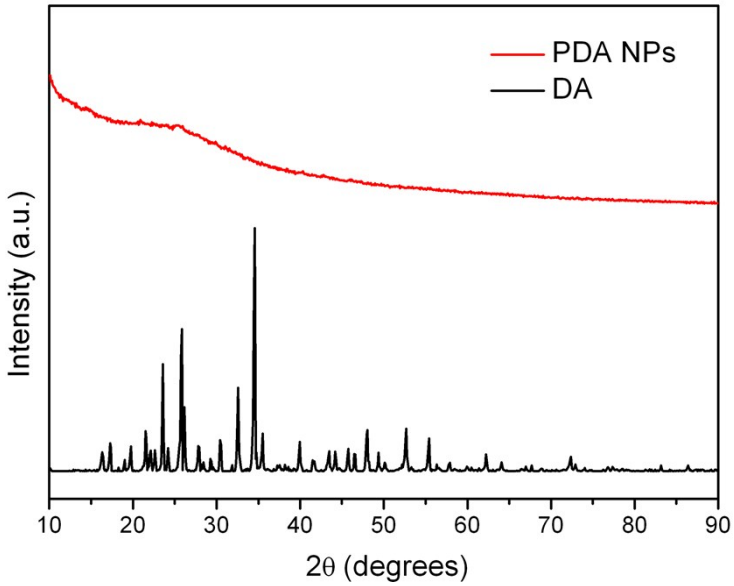

Fig. S6. Powder XRD patterns of PDA NPs and DA·HCl monomers, respectively.

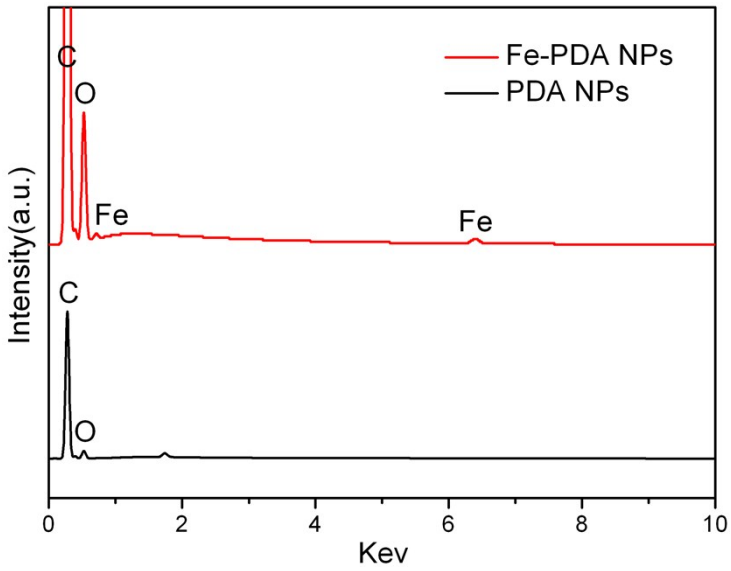

Fig. S7. EDS analysis of Fe-PDA NPs and PDA NPs, respectively.

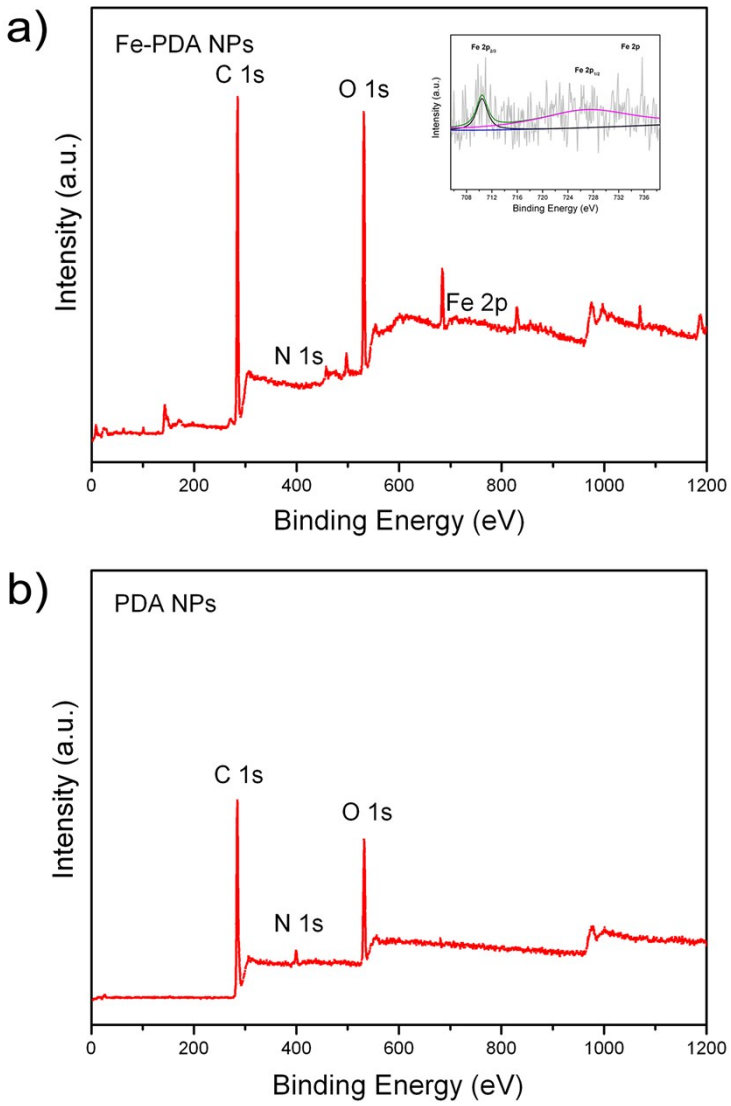

Fig. S8. XPS survey spectra of (a) Fe-PDA NPs and (b) PDA NPs. The insets show the corresponding Fe 2p XPS spectra.

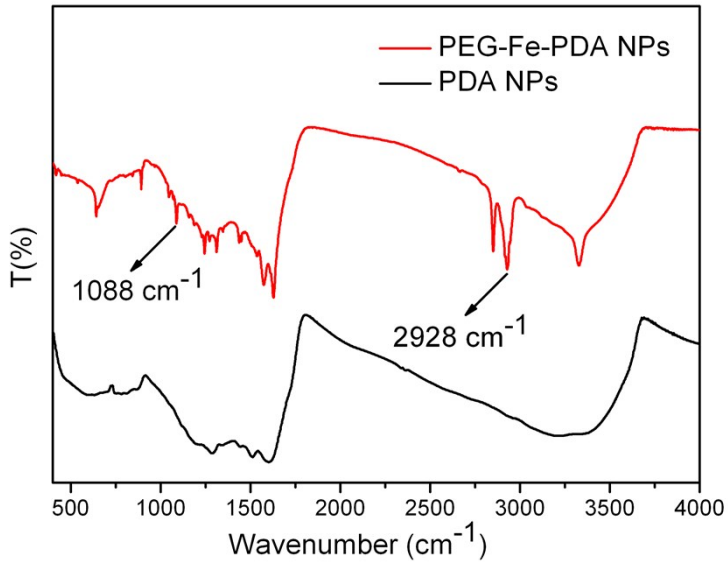

Fig. S9. FT-IR spectra of PEG-Fe-PDA NPs and PDA NPs, respectively.

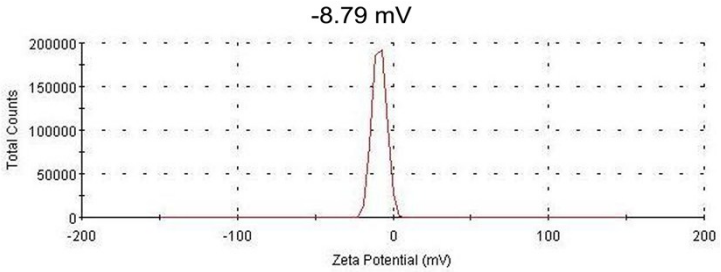

Fig. S10. Zeta Potential measurement of PEG-Fe-PDA NPs.

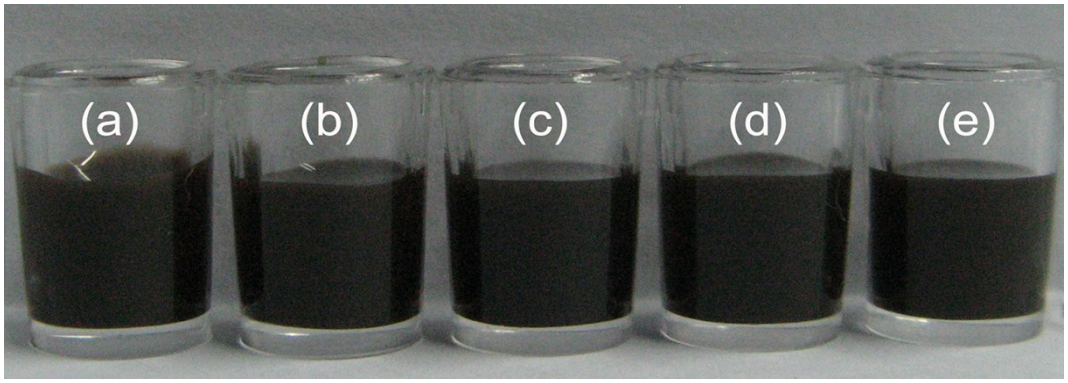

Fig. S11. Dispersibility of PEG-Fe-PDA NPs in different dispersing media including (a) H_2O, (b) PBS (pH=7.4), (c) TB (pH=8.5), (d) 0.9% NaCl solution and (e) DMEM supplemented with 10% FBS (v/v), respectively.

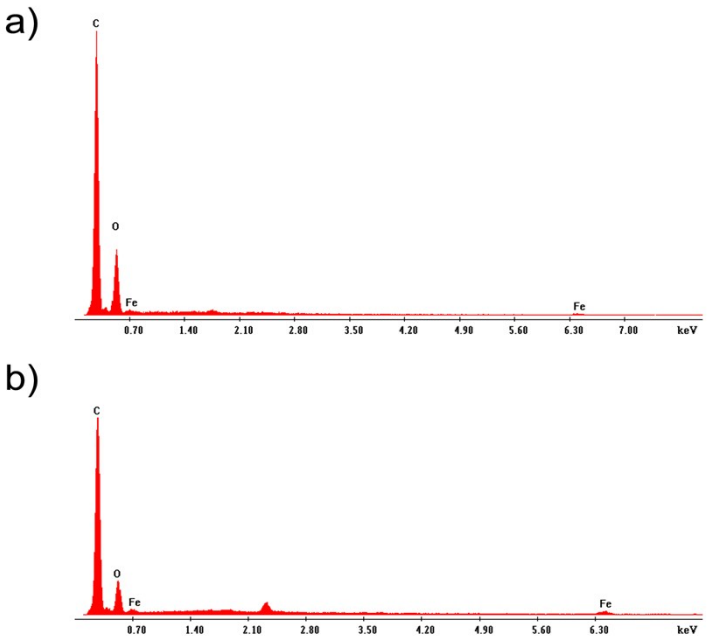

Fig. S12. EDS analysis of Fe-PDA NPs (a) before treatment, (b) after incubated in serum for one week.

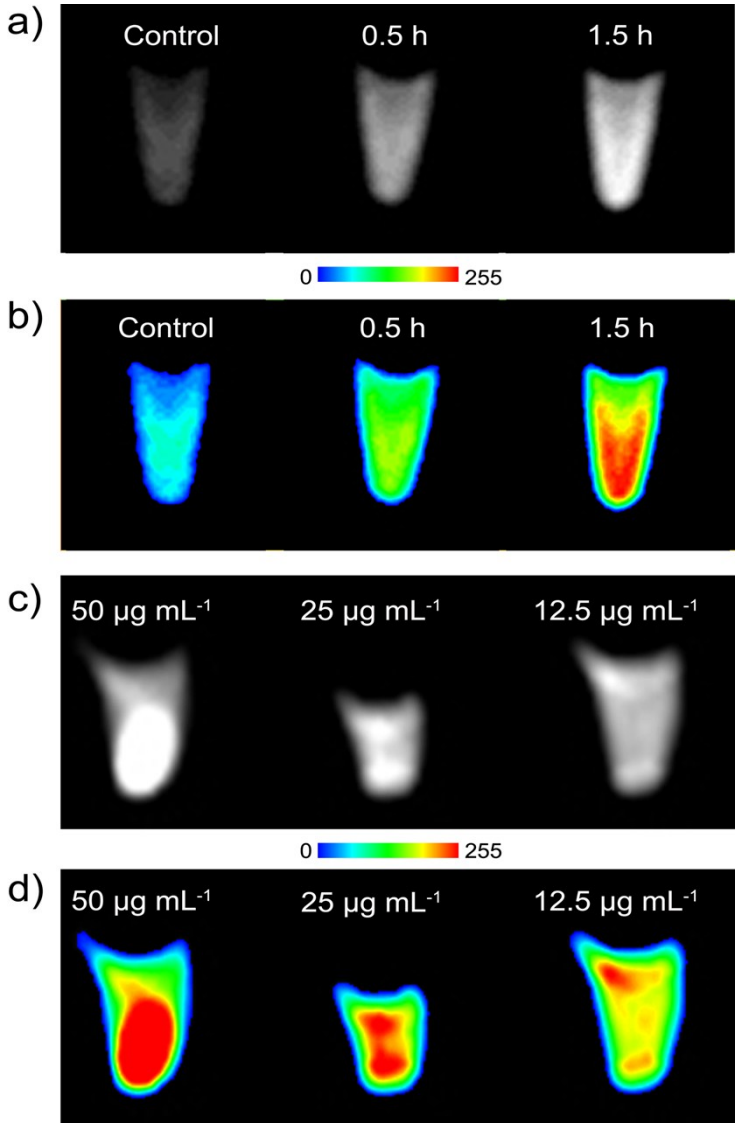

Fig. S13. (a, b) MRI images of PEG-Fe-PDA NPs (50 μg mL^{-1}) stained SW620 cells with different incubation time. (c, d) MRI images of PEG-Fe-PDA NPs stained SW620 cells at different concentration after incubated for 12 h. Corresponding unstained cells were employed as control samples.

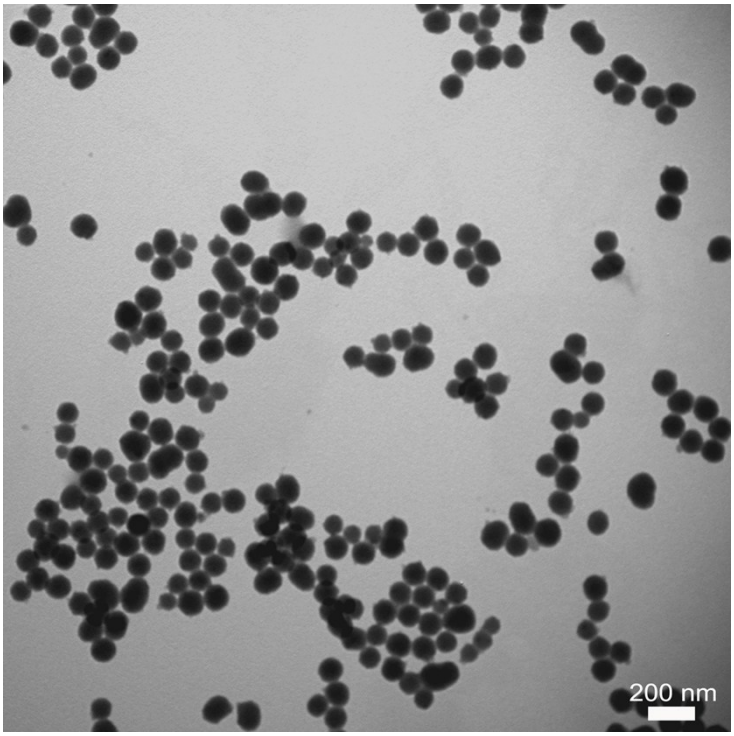

Fig. S14. TEM micrograph of PEG-Fe-PDA NPs (100 nm in diameter).

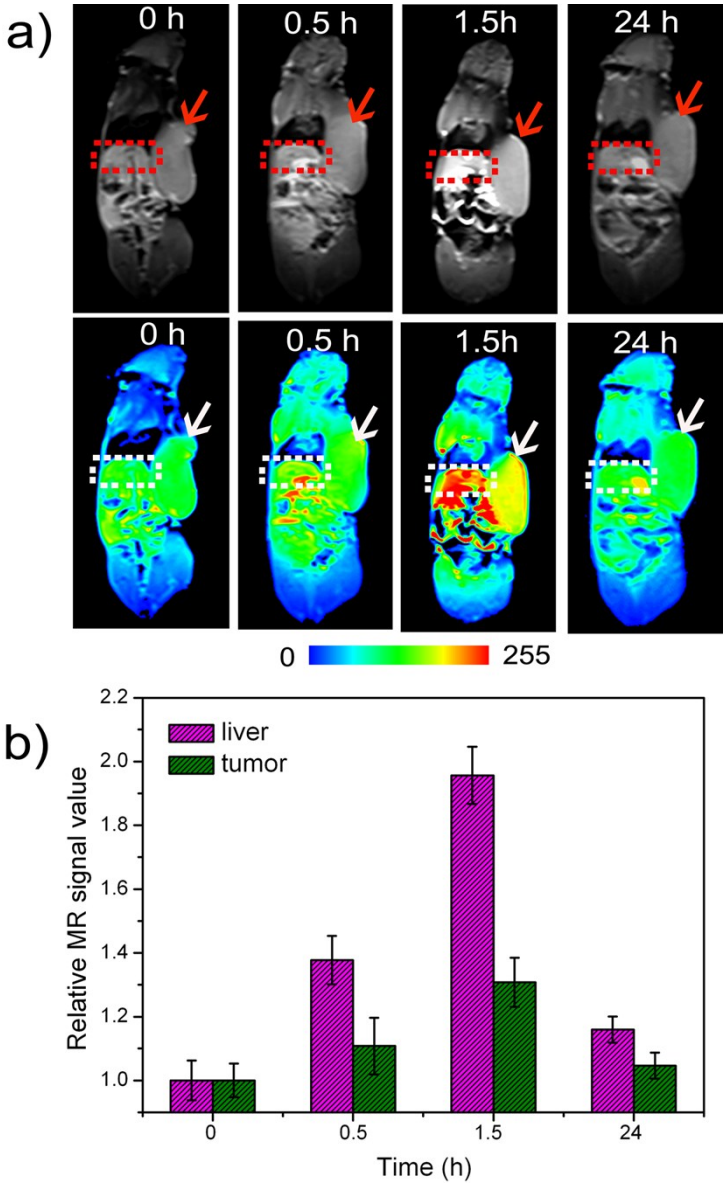

Fig. S15. (a) *In vivo* MR images of nude mice bearing colorectal tumor after intravenous injection (tumor, arrows; liver, rectangles) of PEG-Fe-PDA NPs (100 nm in diameter) at different time intervals (The time 0 h means pre-injection.). (b) Corresponding data analysis of tumor and liver in (a). Error bars mean standard deviations (n=5).

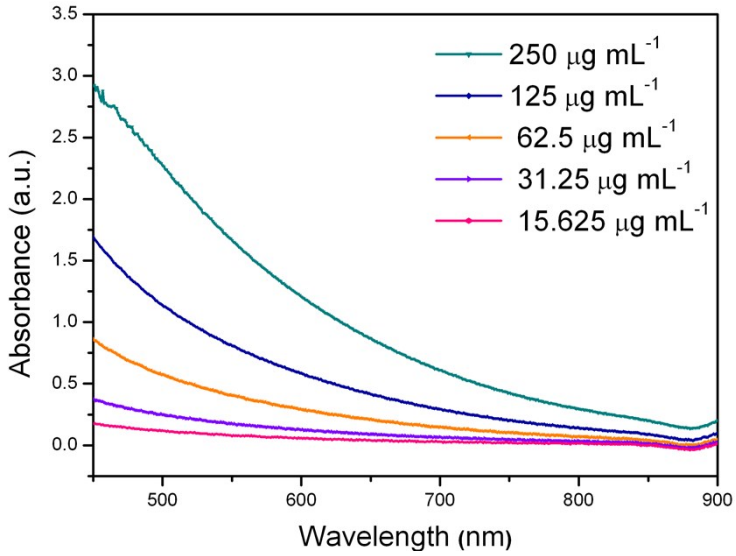

Fig. S16. UV-visible spectra of PEG-Fe-PDA NPs with various concentrations.

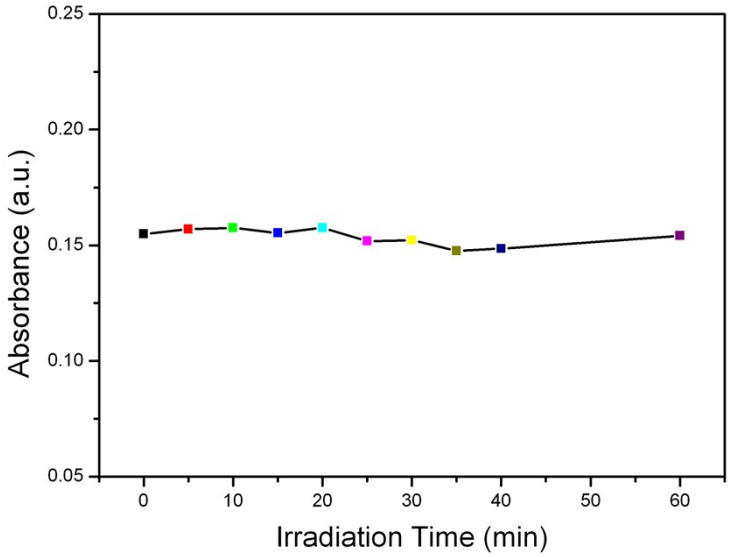

Fig. S17. The absorbance of 150 μg mL^{-1} PEG-Fe-PDA NPs at 808 nm as a function of 808 nm NIR laser irradiation time.

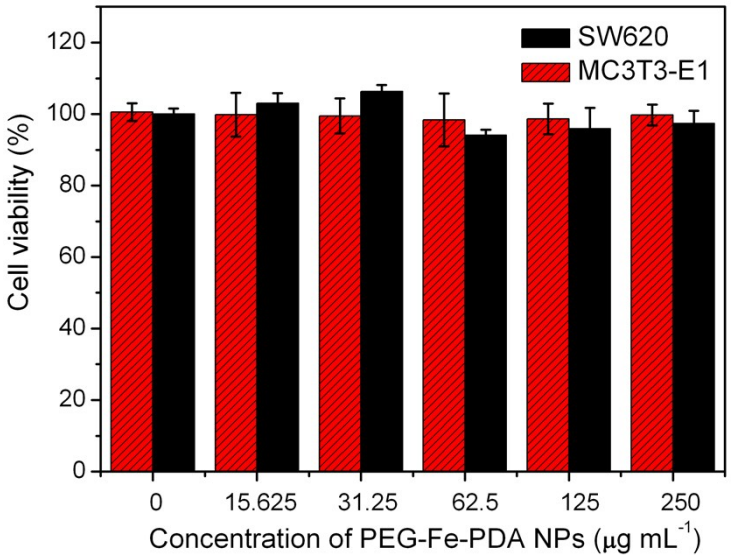

Fig. S18. Cell viabilities of SW620 and MC3T3-E1 cells after incubated with various concentrations of PEG-Fe-PDA NPs. Error bars mean standard deviations (n=5).

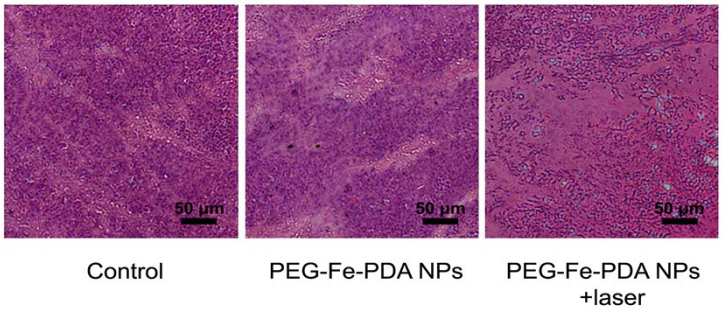

Fig. S19. Histological analysis (Hematoxylin and eosin (H&E) staining) of tumor tissues were collected from mice after different treatments.

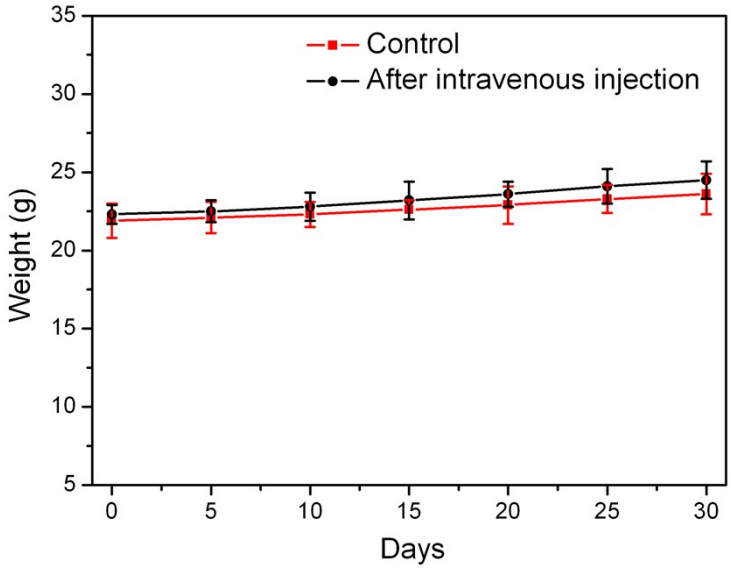

Fig. S20. Body weight changes of the mice with and without intravenous injection of PEG-Fe-PDA NPs versus time.

Additional Table S1. Blood biochemical assay and hematology analysis.

Test	Units	Control (mean±sd)	Treatment (mean±sd)
Biochemistry			
AST	U/L	148.9±18.71	152.8±26.33
ALT	U/L	43.3±6.13	45.7±5.29
TP	g/L	73.7±2.11	72.1±1.87
BUN	mmol/L	6.35±2.12	6.51±1.83
CRE	μmol/L	39.2±3.39	40.5±2.98
Hematological			
WBC	$\times 10^9$/L	11.75±1.27	11.83±1.68
RBC	$\times 10^{12}$/L	9.52±0.91	9.53±0.85
HGB	g/L	167±1.23	166±1.57
LY	%	69.8±6.87	67.3±3.56
MCH	pg	17.50±1.43	17.40±2.64
MCHC	g/L	317.00±6.69	311.00±5.31
MCV	fL	55.50±2.03	54.90±3.18
PLT	$\times 10^9$/L	780.23±45.23	778.38±44.18
PDW	fL	8.80±0.63	8.90±0.98

Additional Table S2. DLS and Zeta Potential analysis of NPs.

NPs	hydrodynamic diameter (nm)	polydispersity index	ζ-potential (mV)
PDA	32.95±3.2	0.20	-46.3±8.89
Fe-PDA	35.87±1.1	0.14	-38.5±8.02
PEG-Fe-PDA	48±1.3	0.18	-8.79±0.51